Differential Binding of Co(II) and Zn(II) to Metallo-β-Lactamase Bla2 from *Bacillus anthracis*

Megan J. Hawk,[1] Robert M. Breece,[2] Christine E. Hajdin,[1] Katherine M. Bender,[1] Zhenxin Hu,[1] Alison L. Costello,[2] Brian Bennett,[3] David L. Tierney,[2*] and Michael W. Crowder[1*]

[1]*Department of Chemistry and Biochemistry, 160 Hughes Hall, Miami University, Oxford, Ohio 45056,*

[2]*Department of Chemistry and Chemical Biology, B80 Clark Hall, MSC03 2060, University of New Mexico, Albuquerque, New Mexico 87131-0001*

[3]*National Biomedical EPR Center, Department of Biophysics, Medical College of Wisconsin, 8701 Watertown Plank Road, Milwaukee, Wisconsin 53226-0509*

Supporting Information

Experimental Procedures

Materials. The pET24bOmpA-Bla2 over-expression plasmid was generously supplied by Professor Timothy Palzkill of the Baylor School of Medicine,[1] and *E. coli* strain BL21(DE3) was purchased from Novagen, Madison, WI. A Minitan II concentrator system was purchased from Fisher Scientific, Pittsburgh, PA, with 1000 NMWL plates from Millipore, Bedford, MA. All chromatographic steps were conducted with a fast protein liquid chromatography (FPLC) system purchased from Amersham Pharmacia Biotech. Nitrocefin and cefaclor were purchased from Becton Dickinson and Sigma, respectively. Meropenem and imipenem were donated by Zeneca Pharmaceticals, Wilmington, DE and Merck and Co., Rahway, NJ, respectively.

Over-Expression, Purification, and Biochemical Characterization. The pET24b-OmpA-Bla2 plasmid was transformed into *E. coli* BL21(DE3) cells via electroporation. Colonies from the transformation were used to inoculate 10 ml of LB medium containing 25 μg/ml kanamycin, and the culture was shaken overnight at 37° C. The overnight culture was used to inoculate 4x1L of LB medium containing 25 μg/ml kanamycin at 37° C, and the culture was shaken at 37° C until reaching an optical density at 600 nm of 0.75-0.85. Protein production was induced with 1 mM isopropyl-β-*D*-thiogalactopyranoside (IPTG), and the cultures were allowed to shake overnight at 25° C.

The resulting cells were centrifuged (10 min at 7500 xg), and the supernatant was collected. The protein solution was kept on ice and concentrated with a Minitan II system equipped with 1000 NMWL plates until the volume reached *ca.* 50 ml. The concentrated protein mixture was centrifuged (30 min at 14500 xg), and the supernatant was dialyzed versus 2L of 50 mM Hepes, pH 6.5, overnight at 4° C. The supernatant was centrifuged

(30 min at 14,500 xg) to remove insoluble matter and loaded onto an SP-Sepharose column (25 ml bed volume), which was pre-equilibrated with 50 mM Hepes, pH 6.5. Bound proteins were eluted with a 0-1 M NaCl gradient in 50 mM Hepes, pH 6.5, at 2 ml/min. Fractions (6 ml) containing Bla2, as determined by SDS-PAGE, were pooled and concentrated with an Amicon ultrafiltration cell equipped with a YM-10 membrane. SDS-PAGE gels (Figure S1) were used to ascertain protein purity. The molecular mass of recombinant Bla2 in 50 mM Hepes, pH 6.5, was determined by MALDI-TOF mass spectrometry. Amino acid analyses of Bla2 were conducted by the Protein Separation and Analysis Laboratory at Purdue University, West Lafayette, IN.

Previously, Palzkill and co-workers had designed a pET24-based over-expression plasmid that produces an OmpA-Bla2 fusion protein.[1] The fusion protein is ultimately exported to the outer membrane, where cleavage of the fusion protein deposits recombinant Bla2 directly into the growth medium. Using our procedure, 17-23 mg of > 95 % pure Bla2 can be obtained from 1 liter of LB medium (Figure S1). Amino acid analyses indicate an extinction coefficient (ε_{280nm}) of 25,400 $M^{-1}cm^{-1}$, and MALDI-TOF MS exhibits an m/z of 25,152 amu (25,360 predicted, based on the amino acid sequence).[2] Metal analysis demonstrates the as-isolated enzyme contains 1.0 $\pm$ 0.2 equivalents of Zn and < 0.1 equivalent of Co, Cu, Ni, Mn, or Fe. Incubation of the as-isolated enzyme with a 4-fold excess of Zn(II), followed by Chelex treatment to remove unbound and loosely bound metal ions, resulted in an enzyme that tightly bound 1.4 $\pm$ 0.1 eq of Zn. In general, the presence of excess Zn(II) in the medium destabilized the dilute enzyme, often resulting in irreversible precipitation; similar effects were not observed at higher (> 0.5 mM) concentrations.

Preparation of apo-Bla2. Bla2 (1-2 ml of 1 mM as-isolated enzyme) was dialyzed versus 4x2L (12 hours each) of 15 mM Hepes, pH 6.5, containing 10 mM EDTA at 4° C. EDTA was removed by dialysis versus 2x2L of Chelex-treated, 15 mM Hepes, pH 6.5, containing 150 mM NaCl, followed by 2x2L of Chelex-treated 15 mM Hepes, pH 6.5, containing 100 mM NaCl, for 6 h each, at 4° C. After the final dialysis step, the protein solution was centrifuged (30 min at 14,500 xg) to remove precipitated protein and then concentrated by ultrafiltration to 1-2 ml. The resulting solution was passed through a Sephadex G-25 column, using Chelex-treated 15 mM Hepes, pH 6.5, containing 100 mM NaCl, as eluent. Fractions were collected, and samples containing Bla2 were pooled and concentrated, prior to the determination of metal content by ICP-AES.

Metal Analyses. The metal content of Bla2 was determined using a Varian Liberty 150 inductively coupled plasma spectrometer with atomic emission detection (ICP-AES). Bla2 samples were diluted to 10 μM or 20 μM in 50 mM Hepes, pH 6.5. Calibration curves of five standards (Zn(II), Cu(II), Ni(II), Mn(II), Co(II), and Fe) were used to quantify the metal ion concentrations in Bla2 samples, as previously reported.[3]

Figure S1. SDS-PAGE gel of purification of recombinant Bla2. Lane 1: molecular weight markers (from top to bottom: 150 kDa, 100 kDa, 75 kDa, 50 kDa, 35 kDa, 25 kDa, and 15 kDa); Lane 2: boiled fraction before induction with IPTG; Lane 3: soluble fraction after dialysis against 50 mM Hepes, pH 6.5; Lane 4: purified Bla2 after SP-Sepharose chromatography.

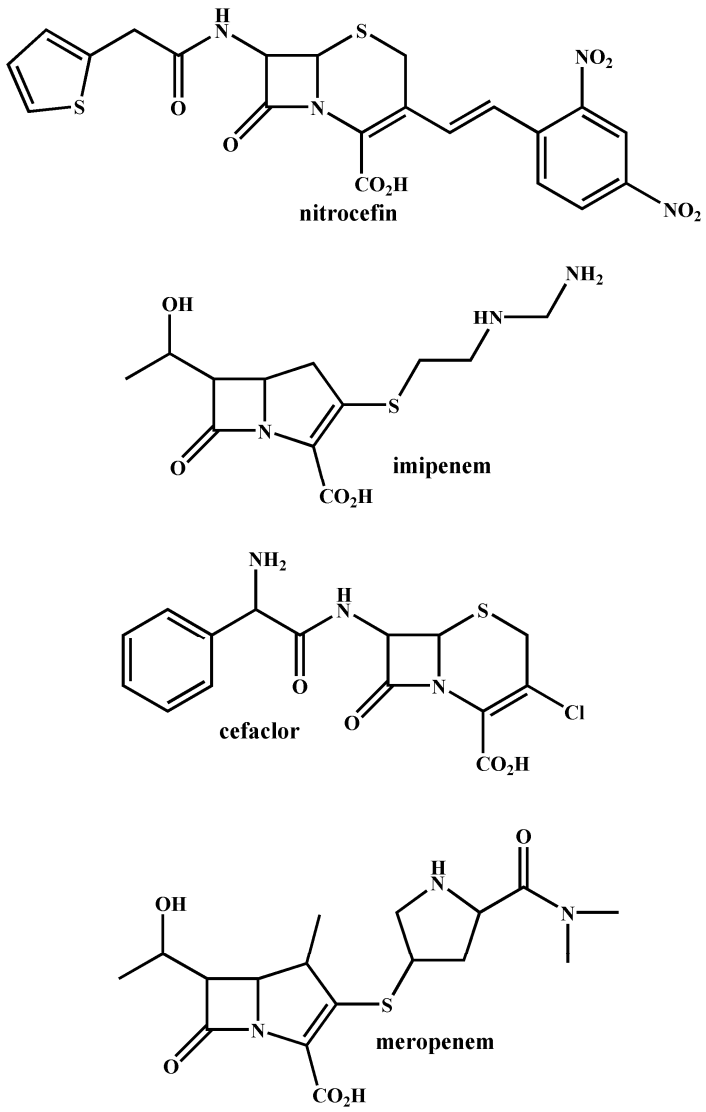

Figure S2. Structures of substrates used in steady-state kinetic studies.

XAS of Zn- and Co-containing Bla2

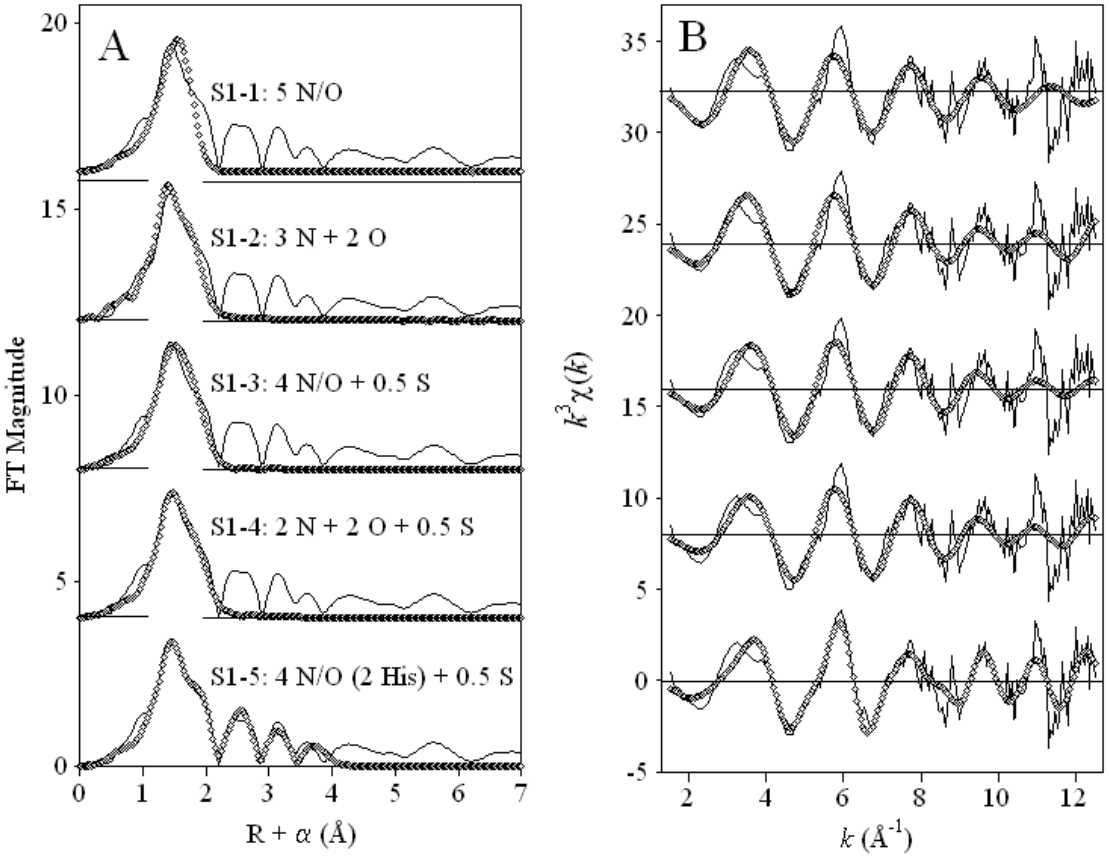

Figure S3. Fourier transforms (A) of k^3-weighted EXAFS (B) for 1Co-Bla2 (solid lines), and corresponding curve fits (open symbols) from Table S1, numbers correspond to entries in the associated Table.

Table S1. Detailed EXAFS curve fitting results for 1Co-Bla2.[a]

Fit	Model	*Co-N/O*	*Co-S*	*Co-His* [b]	*Co-Co*	R_f [c]	R_u [c]
S1-1	5 N/O	2.04 (9.0)				183	428
S1-2	3 N + 2 O	[N] 2.10 (1.0) [O] 1.95 (6.0)				67	353
S1-3	4 N/O + 0.5 S	2.04 (9.0)	2.27 (1.8)			54	355
S1-4	2 N + 2 O + 0.5 S	[N] 2.04 (1.1) [O] 1.90 (5.8)	2.27 (3.8)			31	329
S1-5	4 N/O (2His) + 0.5 S [d]	2.03 (6.9)	2.27 (2.8)	2.91 (4.6), 3.26 (11) 4.01 (5.8), 4.21 (13)		117	188
S1-6	4 N/O (2His) + 0.5 S + Co-Co [d]	2.03 (6.9)	2.27 (3.7)	2.91 (8.6), 3.25 (20) 4.02 (10), 4.21 (14)	3.55 (6.0)	108	168

[a] Distances (Å) and disorder parameters (in parentheses, σ^2 (10^{-3} Å^2)) shown derive from integer or half-integer coordination number fits to filtered EXAFS data [k = 1.5-12.5 Å^{-1}; R = 0.7-2.3 Å (fits 1-4) or 0.2-4.2 Å (fits 5-6)].

[b] Multiple scattering paths represent combined paths, as described previously (see Materials and Methods).

[c] Goodness of fit (R_f for fits to filtered data; R_u for fits to unfiltered data) defined as

$$1000 * \frac{\sum_{i=1}^{N} \left\{ \left[\mathrm{Re}(\chi i_{calc}) \right]^2 + \left[\mathrm{Im}(\chi i_{calc}) \right]^2 \right\}}{\sum_{i=1}^{N} \left\{ \left[\mathrm{Re}(\chi i_{obs}) \right]^2 + \left[\mathrm{Im}(\chi i_{obs}) \right]^2 \right\}}$$

, where N is the number of data points.

[d] Inclusion of a Co-C scattering path (0.5 C/Co), along with the parameters of this fit, led to a refined Co-C distance of 2.42 Å (σ^2 = 0.1 x 10^{-3} Å^2), with a modest decrease in fit residual to R_f = 102.

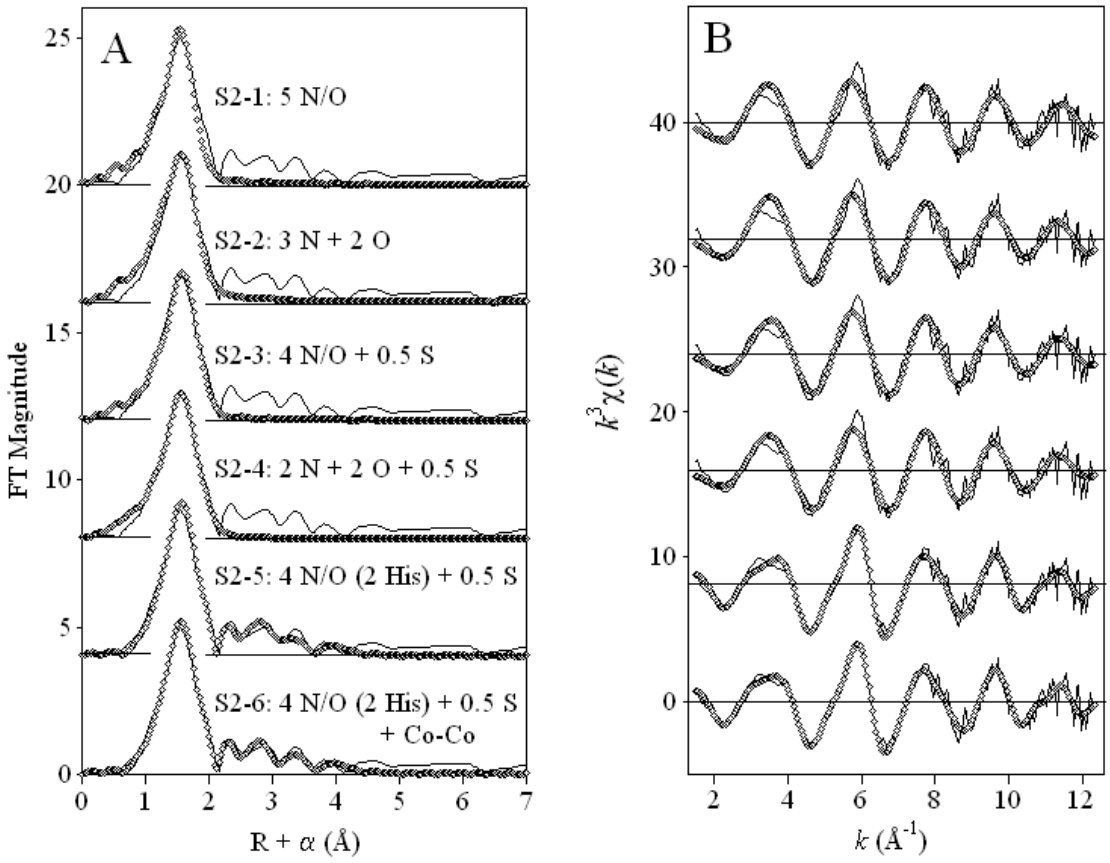

Figure S4. Fourier transforms (A) of k^3-weighted EXAFS (B) for CoCo-Bla2 (solid lines), and corresponding curve fits (open symbols) from Table S2.

Table S2. Detailed EXAFS curve fitting results for CoCo-Bla2.[a]

Fit	Model	*Co-N/O*	*Co-S*	*Co-His* [b]	*Co-Co*	R_f [c]	R_u [c]
S2-1	5 N/O	2.06 (4.2)				39	182
S2-2	3 N + 2 O	[N] 2.09 (1.5) [O] 1.96 (1.4)				20	168
S2-3	4 N/O + 0.5 S	2.05 (3.8)	2.27 (3.2)			12	160
S2-4	2 N + 2 O + 0.5 S	[N] 2.10 (6.0) [O] 1.99 (3.2)	2.27 (1.4)			11	155
S2-5	4 N/O (2His) + 0.5 S[d]	2.05 (3.6)	2.27 (3.5)	2.91 (3.6), 3.29 (18) 3.85 (10), 4.17 (17)		82	107
S2-6	4 N/O (2His) + 0.5 S + Co-Co	2.05 (3.3)	2.27 (3.4)	2.91 (3.7), 3.28 (21) 3.84 (11), 4.16 (19)	3.31 (13)	66	103

[a] Distances (Å) and disorder parameters (in parentheses, σ^2 (10^{-3} Å^2)) shown derive from integer or half-integer coordination number fits to filtered EXAFS data [k = 1.5-12.4 Å^{-1}; R = 0.7-2.3 Å (fits 1-4) or 0.2-4.2 Å (fits 5-6)].

[b] Multiple scattering paths represent combined paths, as described previously (see Materials and Methods).

[c] Goodness of fit (R_f for fits to filtered data; R_u for fits to unfiltered data) defined as

$$1000 * \frac{\sum_{i=1}^{N} \left\{ \left[\mathrm{Re}(\chi i_{calc}) \right]^2 + \left[\mathrm{Im}(\chi i_{calc}) \right]^2 \right\}}{\sum_{i=1}^{N} \left\{ \left[\mathrm{Re}(\chi i_{obs}) \right]^2 + \left[\mathrm{Im}(\chi i_{obs}) \right]^2 \right\}}$$

, where N is the number of data points.

[d] Addition of a Co-C scattering path (0.5 C/Co) to the parameters of this fit led to a refined Co-C distance of 2.43 Å (σ^2 = 0.1 x 10^{-3} Å^2), with a minimal decrease in fit residual to R_f = 78.

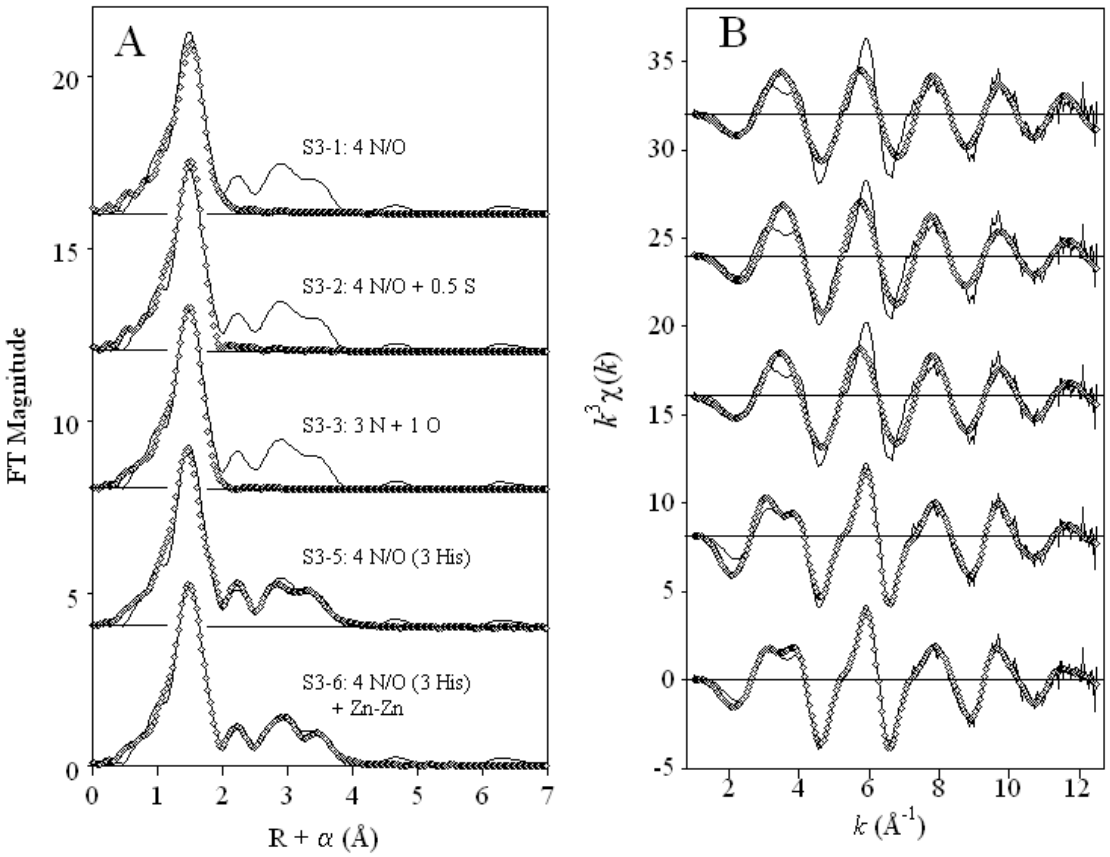

Figure S5. Fourier transforms (A) of k^3-weighted EXAFS (B) for 1Zn-Bla2 (solid lines), and corresponding curve fits (open symbols) from Table S3.

Table S3. Detailed EXAFS curve fitting results for 1Zn-Bla2.[a]

Fit	Model	*Zn-N/O*	*Zn-S*	*Zn-His* [b]	*Zn-Zn*	R_f [c]	R_u [c]
S3-1	4 N/O	2.02 (4.8)				56	200
S3-2	4 N/O + 0.5 S	2.01 (5.0)	2.23 (15)			40	191
S3-3	3 N + 1 O	[N] 2.06 (3.1) [O] 1.93 (1.1)				43	192
S3-4	2 N + 2 N	[N_1] 2.08 (0.5) [N_2] 1.96 (0.1)				46	192
S3-5	4 N/O (3 His)[d]	2.03 (6.6)		2.91 (6.6), 3.16 (9.8) 4.11 (19), 4.42 (23)		40	52
S3-6	4 N/O (3 His) + Zn-Zn	2.03 (6.6)		2.92 (8.6), 3.19 (32) 4.15 (14), 4.39 (20)	3.36 (10)	33	46

[a] Distances (Å) and disorder parameters (in parentheses, σ^2 (10^{-3} Å^2)) shown derive from integer or half-integer coordination number fits to filtered EXAFS data [k = 1.5-12.5 Å^{-1}; R = 0.7-2.2 Å (fits 1-4) or 0.2-4.2 Å (fits 5-6)].

[b] Multiple scattering paths represent combined paths, as described previously (see Materials and Methods).

[c] Goodness of fit (R_f for fits to filtered data; R_u for fits to unfiltered data) defined as

$$1000 * \frac{\sum_{i=1}^{N}\left\{\left[\mathrm{Re}(\chi i_{calc})\right]^2 + \left[\mathrm{Im}(\chi i_{calc})\right]^2\right\}}{\sum_{i=1}^{N}\left\{\left[\mathrm{Re}(\chi i_{obs})\right]^2 + \left[\mathrm{Im}(\chi i_{obs})\right]^2\right\}}$$

, where N is the number of data points.

[d] Inclusion of a Zn-C scattering path (0.5 C/Zn), along with the parameters of this fit, led to a refined Zn-C distance of 2.55 Å (σ^2 = 5.3 x 10^{-3} Å^2), with a modest decrease in fit residual to R_f = 36.

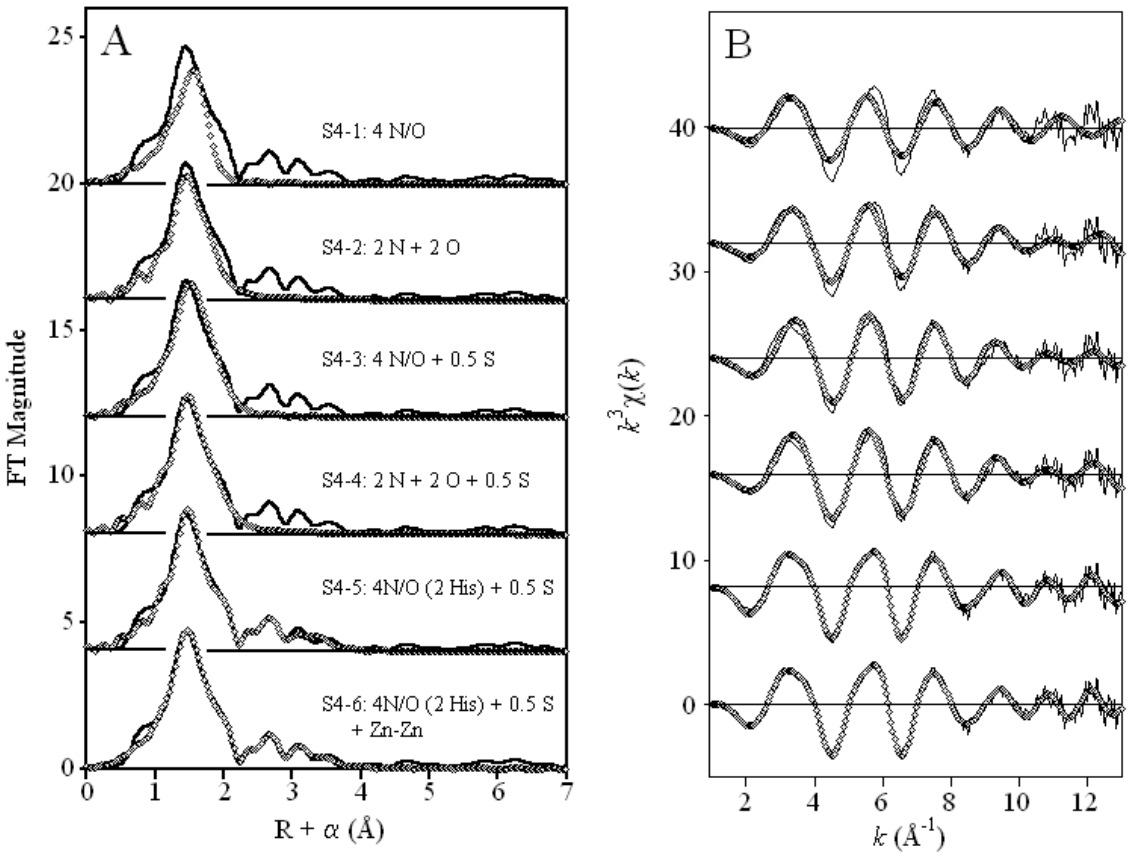

Figure S6. Fourier transforms (A) of k^3-weighted EXAFS (B) for ZnZn-Bla2 (solid lines), and corresponding curve fits (open symbols) from Table S4.

Table S4. Detailed EXAFS curve fitting results for ZnZn-Bla2.[a]

Fit	Model	*Zn-N/O*	*Zn-S*	*Zn-His* [b]	*Zn-Zn*	R_f [c]	R_u [c]
S4-1	4 N/O	2.07 (6.5)				186	230
S4-2	2 N + 2 O	[N] 2.13 (0.1) [O] 1.98 (1.7)				55	127
S4-3	4 N/O + 0.5 S	2.04 (6.4)	2.27 (14)			22	191
S4-4	2 N + 2 O + 0.5 S	[N] 2.14 (6.5) [O] 1.97 (2.9)	2.27 (2.6)			13	96
S4-5	4 N/O (2His) + 0.5 S [d]	2.04 (6.5)	2.27 (2.6)	2.90 (7.6), 3.10 (3.8) 4.09 (17), 4.43 (25)		21	56
S4-6	4 N/O (2His) + 0.5 S + Zn-Zn [e]	2.04 (6.3)	2.27 (2.6)	2.90 (7.1), 3.08 (5.8) 4.08 (18), 4.43 (25)	3.44 (15)	9	36

[a] Distances (Å) and disorder parameters (in parentheses, σ^2 (10^{-3} Å^2)) shown derive from integer or half-integer coordination number fits to filtered EXAFS data [k = 1-13 Å^{-1}; R = 0.7-2.3 Å (Fits 1-4) or 0.2-4.2 Å (Fits 5-6)].

[b] Multiple scattering paths represent combined paths, as described previously (see Materials and Methods).

[c] Goodness of fit (R_f for fits to filtered data; R_u for fits to unfiltered data) defined as

$$1000 * \frac{\sum_{i=1}^{N} \left\{ \left[\mathrm{Re}(\chi i_{calc}) \right]^2 + \left[\mathrm{Im}(\chi i_{calc}) \right]^2 \right\}}{\sum_{i=1}^{N} \left\{ \left[\mathrm{Re}(\chi i_{obs}) \right]^2 + \left[\mathrm{Im}(\chi i_{obs}) \right]^2 \right\}}$$

, where N is the number of data points.

[d] Addition of a Zn-C scattering path (0.5 C/Zn) to the parameters of this fit led to a refined Zn-C distance of 2.55 Å (σ^2 = 5.3 x 10^{-3} Å^2) and minimal improvement in fit residual to R_f = 20.

[e] Addition of a Zn-C scattering path (0.5 C/Zn) to the parameters of this fit led to a refined Zn-C distance of 2.51 Å (σ^2 = 1.3 x 10^{-3} Å^2) and minor improvement in fit residual to R_f = 8.

Zn K-edge XAS of the B1 MβL CcrA.

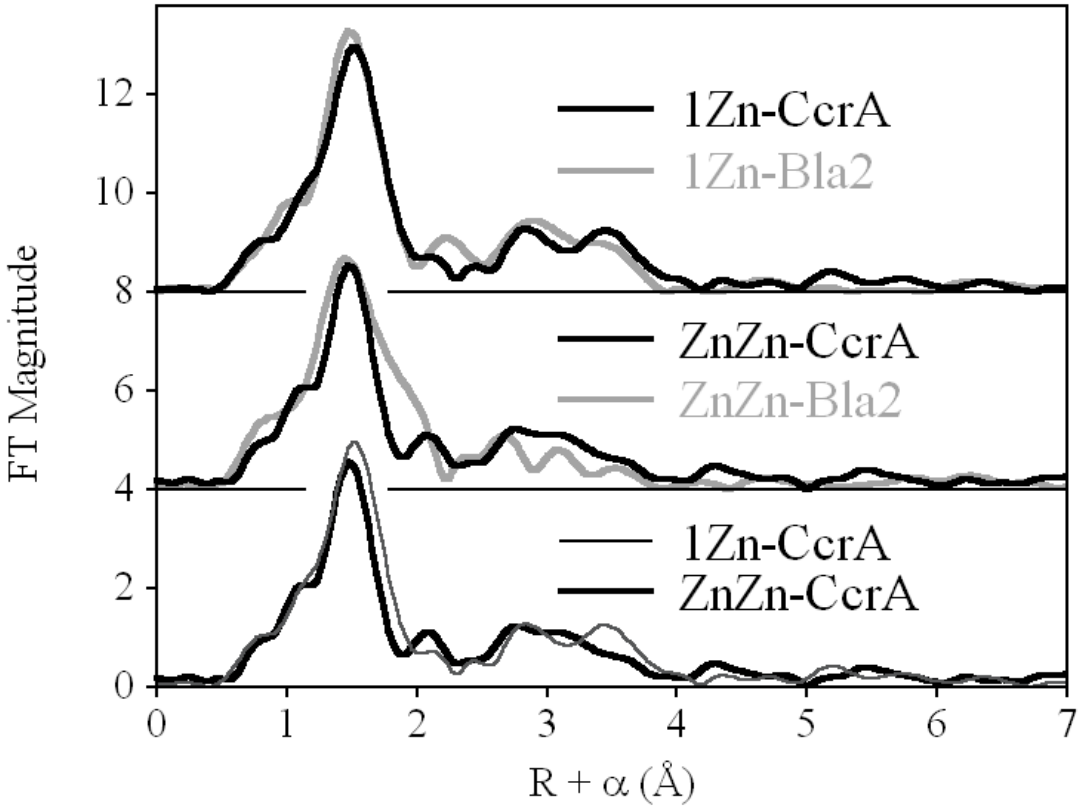

Figure S7. EXAFS Fourier transforms for Zn-CcrA. (Top) Direct comparison of 1Zn-CcrA (black line) and 1Zn-Bla2 (gray line). (Center) Direct comparison of ZnZn-CcrA (black line) and ZnZn-Bla2 (gray line). (Bottom) Direct comparison of 1Zn-CcrA (thin black line) and ZnZn-CcrA (thick black line).

The discrepancy in metal-binding mechanisms followed by Bla2 led us to examine Zn(II) binding by the B1 MβL CcrA from *B. fragilis*. Samples were prepared as described previously,[4] and the data were analyzed in the same fashion as those for Bla2. The metal site in CcrA is analogous to Bla2 and, in light of our previous work on Co binding by CcrA,[4] we expect the same pattern as Zn binding by Bla2 with the first metal ion exclusively populating the Zn_1 site. As can be seen in Figure S7 (Top), the FTs for 1Zn-CcrA and 1Zn-Bla2 are remarkably similar. The similarity of the FTs is reflected in the curve fitting results for 1Zn-CcrA (Table S5 and Figure S8), which are nearly identical to 1Zn-Bla2, including only minimal improvements on (*i*) addition of a partial sulfur scatterer (compare Fits S5-2 and S5-1), (*ii*) using resolved N and O shells (Fits S5-3 and S5-1), or (*iii*) inclusion of a Zn-Zn vector in multiple scattering fits (Fits S5-4 and S5-5).

At first glance, the similarity of Zn-loaded CcrA and Bla2 dissolves on loading the second eq of Zn(II). The main peaks in the EXAFS FTs for ZnZn-CcrA and ZnZn-Bla2 are strikingly different (Figure S7, Center), although the CcrA FT returns nearly to baseline at a point similar to Bla2. The overall curve fitting results (Figure S9 and Table S6) indicate that the apparent difference in their FTs is an artifact of subtle differences in structure. The average first shell bond length increases on addition of a second Zn(II) to CcrA, though not as much as for Bla2, and the best fit with only N/O scatterers indicates an average coordination number of 4 (Fit S6-1). Inclusion of a partial sulfur scatterer improves the fit residual by 48 % (compare Fits S6-2 and S6-1), and this is a well-defined minimum (compare Fits S6-2 and S6-3). Qualitatively, this leads to a much better match

of the main peak's amplitude, with a small shoulder that contributes to the first outer shell peak (Figure S9A), typically ascribed to M-His and/or M-$C_{CO_2^-}$ scattering. The same fit, replacing the Zn-S with a Zn-C scattering path gives only a 32 % improvement (Fit S6-5 vs. Fit S6-1), while inclusion of both leads to an overall 66 % decrease in fit residual (Fit S6-4). The refined Zn-S distance for ZnZn-CcrA is 0.06 Å longer than that obtained for ZnZn-Bla2. Comparison of the combined Zn-S/Zn-C scattering in *k*-space for these two scenarios (see Figure S10) shows that as the Zn-S and Zn-C distances converge, a partial cancellation effect leads to the lack of an obvious Zn-S interaction in the ZnZn-CcrA FT.

Multiple scattering fits for ZnZn-CcrA indicate an average of 2 His ligands per Zn, and inclusion of a Zn-$C_{CO_2^-}$ scattering path (increasing the number of variables from 14-16), leads to a modest 17 % improvement in R_f (compare fits S6-6 and S6-7). In both cases, addition of a Zn-Zn vector leads to ∃50 % improvement in the fit residual (compare Fit S6-6 to Fit S6-8, and Fit S6-7 to Fit S6-9). The refined Zn-Zn distance is, again, fully consistent with those observed for other resting di-Zn MβLs by XAS[5] and diffraction.[6-8]

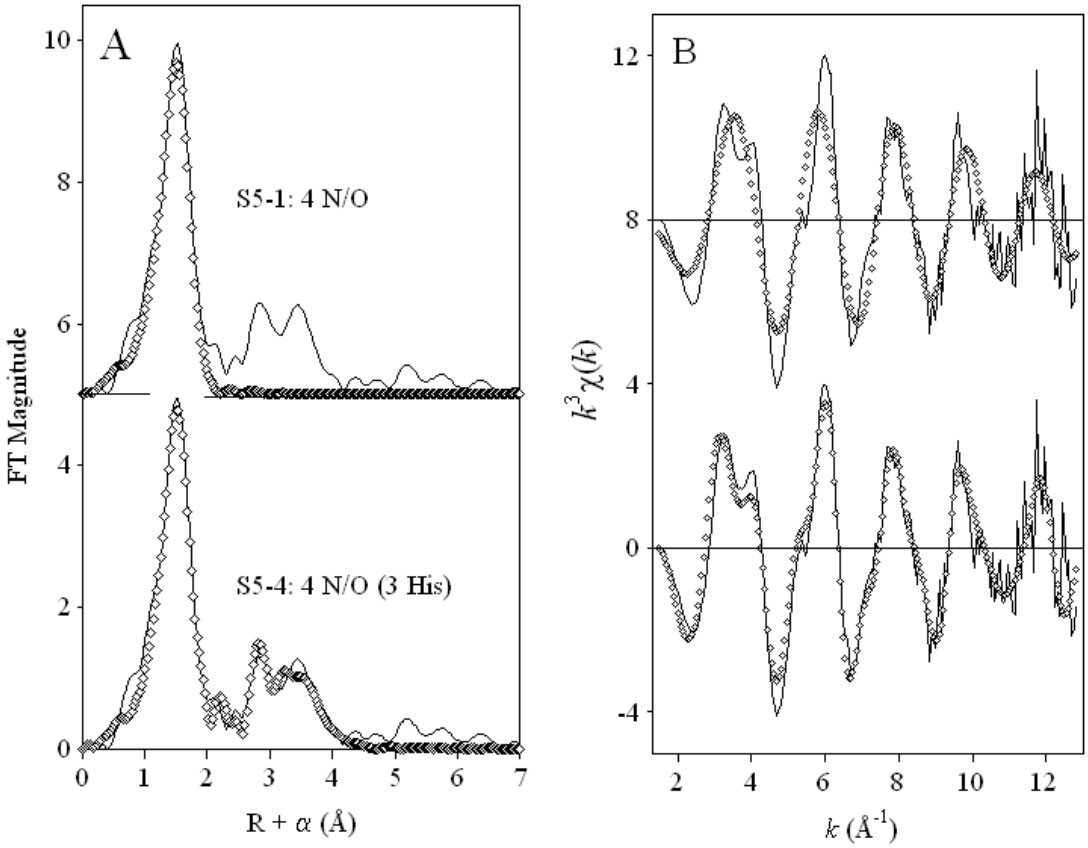

Figure S8. Fourier transforms (A) of k^3-weighted EXAFS (B) for 1Zn-CcrA (solid lines), and corresponding curve fits (open symbols) from Table S5.

Table S5. Detailed EXAFS curve fitting results for 1-Zn CcrA.[a]

Fit	Model	*Zn-N/O*	*Zn-S*	*Zn-His* [b]	*Zn-Zn*	R_f [c]	R_u [c]
S5-1	4 N/O	2.02 (4.6)				55	198
S5-2	4 N/O + 0.5 S	1.99 (6.0)	2.19 (7.2)			41	175
S5-3	3 N + 1 O	[N] 2.03 (2.3) [O] 1.89 (1.8)				42	176
S5-4	4 N/O (3 His)	2.03 (6.9)		2.91 (6.6), 3.16 (9.8) 4.11 (19), 4.42 (23)		26	88
S5-5	4 N/O (3 His) + Zn-Zn	2.03 (6.9)		2.91 (7.6), 3.16 (10) 4.12 (18), 4.41 (21)	3.32 (9.0)	24	88

[a] Distances (Å) and disorder parameters (in parentheses, σ^2 (10^{-3} Å^2)) shown derive from integer or half-integer coordination number fits to filtered EXAFS data [k = 1.5-12.6 Å^{-1}; R = 0.7-2.2 Å (fits 1-3) or 0.2-4.2 Å (fits 4-5)].

[b] Multiple scattering paths represent combined paths, as described previously (see Materials and Methods).

[c] Goodness of fit (R_f for fits to filtered data; R_u for fits to unfiltered data) defined as

$$1000 * \frac{\sum_{i=1}^{N} \left\{ \left[\mathrm{Re}(\chi i_{calc}) \right]^2 + \left[\mathrm{Im}(\chi i_{calc}) \right]^2 \right\}}{\sum_{i=1}^{N} \left\{ \left[\mathrm{Re}(\chi i_{obs}) \right]^2 + \left[\mathrm{Im}(\chi i_{obs}) \right]^2 \right\}}$$

, where N is the number of data points.

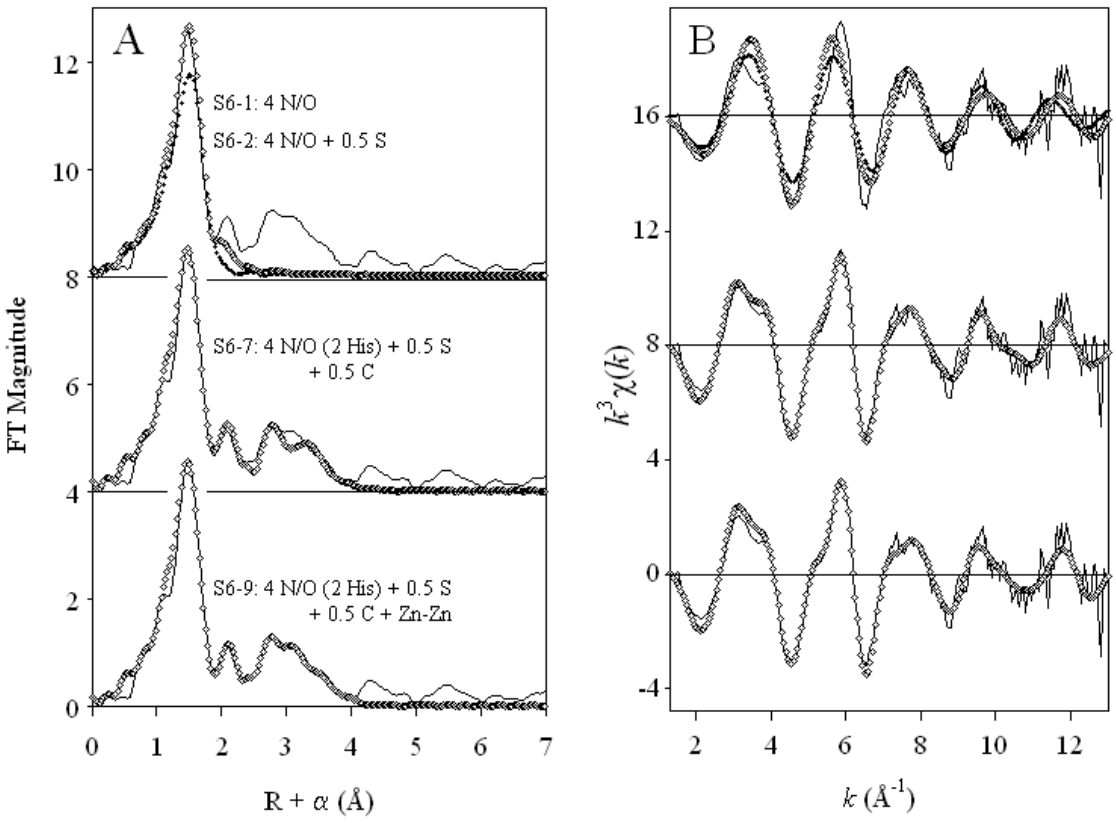

Figure S9. Fourier transforms (A) of k^3-weighted EXAFS (B) for ZnZn-CcrA (solid lines), and corresponding curve fits (open symbols, except S6-1 shown with filled symbols) from Table S6.

Table S6. Detailed EXAFS curve fitting results for ZnZn-CcrA.[a]

Fit	Model	*Zn-N/O*	*Zn-S*	*Zn-C_{CO_2}*	*Zn-His* [b]	*Zn-Zn*	R_f [c]	R_u [c]
S6-1	4 N/O	2.04 (7.0)					125	243
S6-2	4 N/O + 0.5 S	2.02 (6.4)	2.33 (6.0)				65	218
S6-3	4 N/O + 1 S	2.03 (7.6)	2.32 (14)				103	237
S6-4	4 N/O + 0.5 S + 0.5 C	2.03 (6.2)	2.33 (6.6)	2.50 (0.8)			43	207
S6-5	4 N/O + 0.5 C	2.04 (6.8)		2.53 (0.1)			85	221
S6-6	4 N/O (2 His) + 0.5 S	2.03 (6.9)	2.33 (5.2)		2.92 (6.3), 3.17 (3.4) 4.11 (16), 4.42 (20)		54	90
S6-7	4 N/O (2 His) + 0.5 S + 0.5 C	2.03 (6.7)	2.33 (7.8)	2.48 (1.4)	2.91 (7.1), 3.14 (3.3) 4.11 (16), 4.42 (20)		45	79
S6-8	4 N/O (2 His) + 0.5 S + Zn-Zn	2.03 (6.8)	2.33 (5.7)		2.91 (7.6), 3.14 (8.7) 4.17 (23), 4.42 (18)	3.44 (11)	27	65
S6-9	4 N/O (2 His) + 0.5 S + Zn-Zn + 0.5 C	2.03 (5.9)	2.33 (4.5)	2.49 (1.4)	2.91 (6.8), 3.15 (3.5) 4.17 (22), 4.42 (18)	3.44 (11)	21	62

[a] Distances (Å) and disorder parameters (in parentheses, σ^2 (10^{-3} Å^2)) shown derive from integer or half-integer coordination number fits to filtered EXAFS data [k = 1.5-12.5 Å^{-1}; R = 0.7-2.3 Å (fits 1-5) or 0.2-4.2 Å (fits 6-9)].

[b] Multiple scattering paths represent combined paths, as described previously (see Materials and Methods)

[c] Goodness of fit (R_f for fits to filtered data, R_u for fits to unfiltered data) defined as

$$1000 * \frac{\sum_{i=1}^{N} \left\{ \left[\mathrm{Re}(\chi i_{calc}) \right]^2 + \left[\mathrm{Im}(\chi i_{calc}) \right]^2 \right\}}{\sum_{i=1}^{N} \left\{ \left[\mathrm{Re}(\chi i_{obs}) \right]^2 + \left[\mathrm{Im}(\chi i_{obs}) \right]^2 \right\}}$$

, where N is the number of data points.

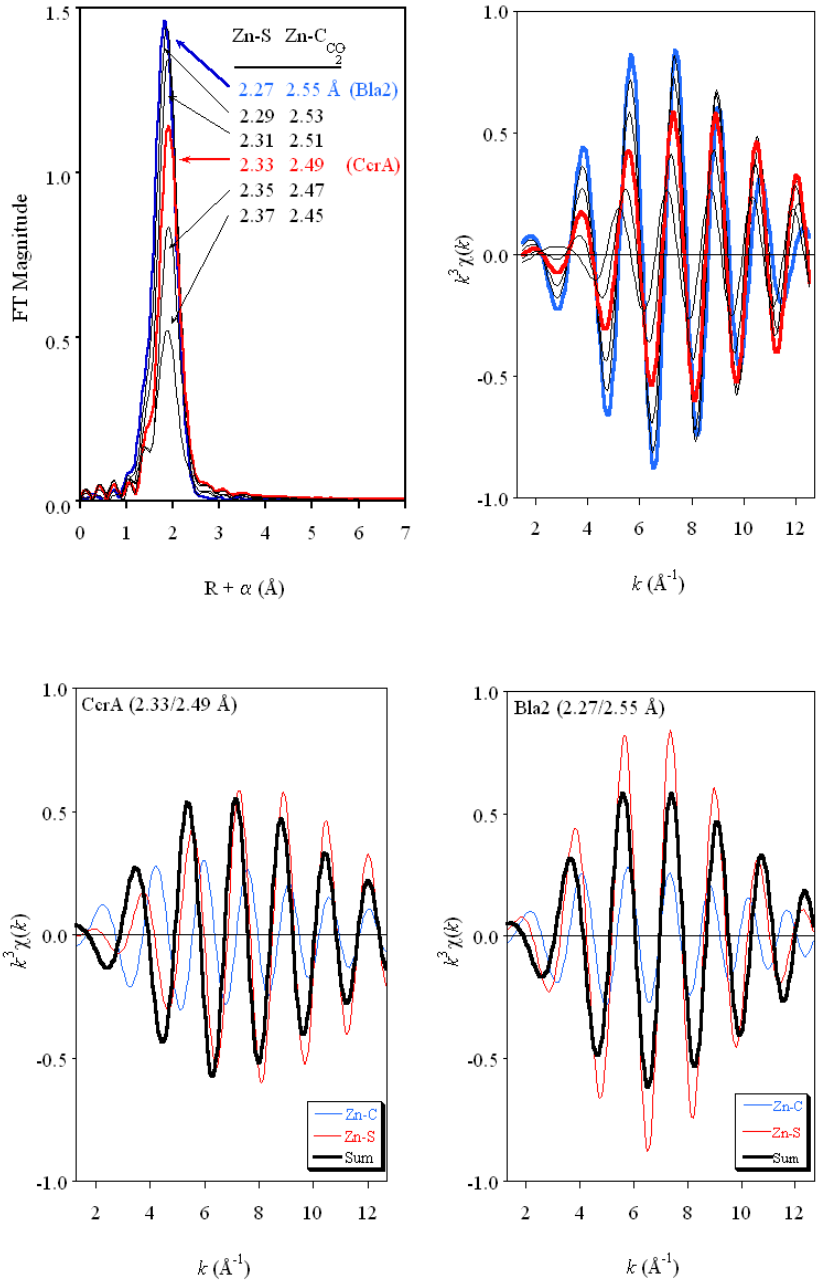

Figure S10. (Top) Simulations demonstrating the effect of convergent Zn-S and Zn-C_{CO_2} distances on their combined EXAFS amplitude; refined values for Bla2 and CcrA are shown in blue and red, respectively. In *k*-space (Top, Right), the effect is most pronounced at low *k*, where Zn-S scattering is most detectable in the EXAFS of metalloproteins sites that also include imidazole ligands. (Bottom) Contributions from individual paths, showing greater phase damping in the CcrA example, where the two distances are closer, particularly in the first two oscillations.

References

1. Materon, I. C.; Queenan, A. M.; Koehler, T. M.; Bush, K.; Palzkill, T., *Antimicrob. Agents Chemother.* **2003**, *47*, 2040-2042.
2. Chen, Y.; Tenover, F. C.; Koehler, T. M., *Antimicrob. Agents Chemother.* **2004**, *48*, 4873-4877.
3. Crowder, M. W.; Walsh, T. R.; Banovic, L.; Pettit, M.; Spencer, J., *Antimicrob. Agents Chemother.* **1998**, *42*, 921-926.
4. Periyannan, G.; Costello, A. L.; Tierney, D. L.; Yang, K. W.; Bennett, B.; Crowder, M. W., *Biochemistry* **2006**, *45*, 1313-1320.
5. Costello, A.; Periyannan, G.; Yang, K. W.; Crowder, M. W.; Tierney, D. L., *J. Biol. Inorg. Chem.* **2006**, *11*, 351-358.
6. Concha, N. O.; Rasmussen, B. A.; Bush, K.; Herzberg, O., *Structure* **1996**, *4*, 823-836.
7. Ullah, J. H.; Walsh, T. R.; Taylor, I. A.; Emery, D. C.; Verma, C. S.; Gamblin, S. J.; Spencer, J., *J. Mol. Biol.* **1998**, *284*, 125-136.
8. Concha, N. O.; Janson, C. A.; Rowling, P.; Pearson, S.; Cheever, C. A.; Clarke, B. P.; Lewis, C.; Galleni, M.; Frere, J. M.; Payne, D. J.; Bateson, J. H.; Abdel-Meguid, S. S., *Biochemistry* **2000**, *39*, 4288-4298.